Charge radii and moments of tin nuclei by laser spectroscopy

M. Anselment,* K. Bekk, A. Hanser, H. Hoeffgen,† G. Meisel, S. Göring, H. Rebel, and G. Schatz
Kernforschungszentrum Karlsruhe, Institut für Kernphysik, D-7500 Karlsruhe, Federal Republic of Germany
(Received 7 April 1986)

The isotope shift and hyperfine structure of the optical Sn I resonance transition $5p^2\ ^3P_0 \rightarrow 5p\,6s\ ^3P_1$ at $\lambda = 286.3$ nm have been studied for 18 Sn nuclei including two isomers. Laser-induced resonance fluorescence from a collimated atomic beam of tin was observed using a tunable continuous wave dye laser with frequency doubler. The electromagnetic nuclear moments and changes of the mean square charge radii of the nuclear charge distributions were determined. The results are discussed with respect to the information they provide on the nuclear structure of the nuclei investigated; they are compared with various theoretical models.

I. INTRODUCTION

The energies of atomic transitions, in particular those associated with s electrons, alter slightly with the neutron number of the atomic nucleus. This isotope shift arises from the difference of the nuclear masses of the isotopes and from the difference of the nuclear Coulomb field experienced by the atomic electrons involved in the transition. The latter contribution, historically referred to as the volume effect,[1] is due to isotopic differences of the nuclear charge distributions of which the mean square charge radius $\langle r^2 \rangle$ enters into the volume effect calculation. Effects of nuclear polarization associated with the interaction between atomic and nuclear states also give rise to isotope shifts, but this contribution is expected to be so small that it can be ignored for transitions of normal atoms.[2] In addition, the interaction of the nuclear magnetism and of nonspherical components of the nuclear charge distribution with the atomic electrons lead to the well-known hyperfine splitting of atomic lines.

Studies of these nuclear effects observed in atomic transitions are an important source of nuclear structure information, in particular about the systematics of nuclear charge radii and electromagnetic moments in long isotopic series. The renewed interest[3–5] in nuclear structure investigations of this kind originates from the progress of experimental techniques, mainly due to the application of laser spectroscopic methods[6] which give enhanced resolution, improved accuracy, and higher sensitivity. In parallel, refined theoretical interpretations of the experimental findings have been developed on the basis of macroscopic[7–9] and microscopic[10–13] structure models accounting even for details in the trend of the nuclear charge radii. The observed trends are globally fairly well described by the droplet model,[7] recently extended by the inclusion of deformation effects[14] which are clearly required by the experimental data (see Ref. 15), e.g., revealing the onset of deformation in new nuclidic regions far from stability.[16] In the neighborhood of magic nuclei (as, e.g., lead[17,18]), where effects of static or dynamic deformations are of reduced importance, there are features (and accordingly, deviations from the droplet model) which originate from the specific shell structure[18–20], and may shed some light on pairing interactions.[13]

The present paper reports on laser spectroscopic measurements of the isotope shift and the hyperfine splitting in the $5p^2\ ^3P_0 \rightarrow 5p6s\ ^3P_1$ resonance transition at $\lambda = 286.3$ nm of stable and radioactive Sn atoms, providing results on a total of 18 nuclei including two isomers. The experiments extend earlier measurements on stable isotopes[21–23] and radio-frequency (rf) studies of radioactive ^{113}Sn and ^{121}Sn; the latter gave results for the values of the nuclear ground state spins and of the electromagnetic moments, though without sign.[24] Recently, the $5p^2\ ^1S_0 \rightarrow 5p\,6s\ ^1P_1$ transition ($\lambda = 452.5$ nm) has been investigated[20] by collinear laser spectroscopy extending our findings to ^{109}Sn and ^{108}Sn.

The specific interest in Sn (which has the highest number of stable isotopes among all elements) arises from the changing polarization of the closed proton shell ($Z = 50$) with the variation of the neutron number between $N = 50$ (i.e., from the experimentally undiscovered doubly magic ^{100}Sn) to $N = 82$ (i.e., the doubly magic ^{132}Sn). In the corresponding case of Ca, the polarization of the proton core is manifested by a rather peculiar variation of the charge radii,[25] showing decreasing values of the mean square charge radii $\langle r^2 \rangle_{\text{charge}}$ when ^{48}Ca is approached. The corresponding ^{132}Sn is inaccessible by present laser spectroscopic methods. From the point of view of the single particle model, however, a subshell closure is expected at $N = 64$. Effects of such subshell closure are also reported for the charge radii of the neighboring element Cd.[26]

II. EXPERIMENTAL ARRANGEMENT

The experimental method applied is laser-induced fluorescence spectroscopy, i.e., free tin atoms, obtained by vacuum evaporation of elementary tin samples, are irradiated with resonant laser light to excite them (see Fig. 1). The resonance absorption is detected indirectly by monitoring the spontaneously reemitted fluorescence light. For

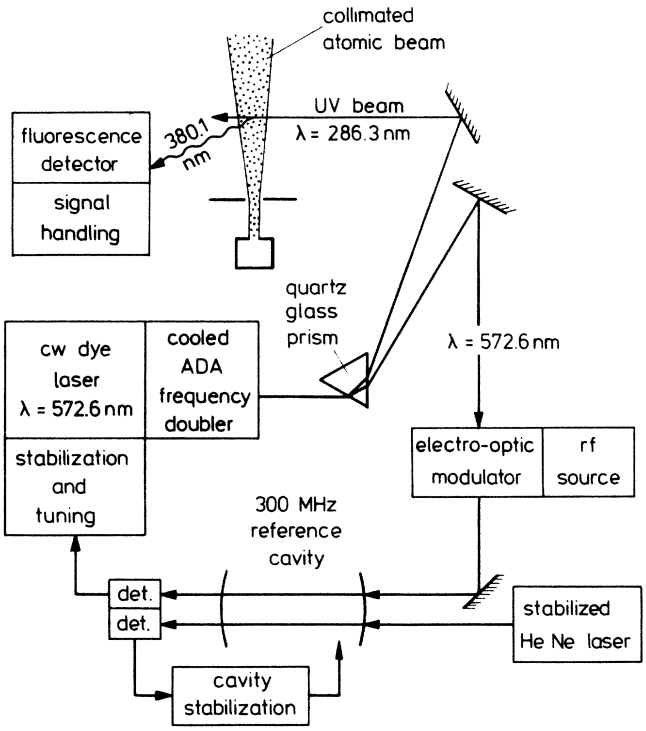

FIG. 1. Schematic diagram of the experimental arrangement.

the light absorption the resonance transition from the ground state $5s^25p^2\ ^3P_0$ to the $5s^25p6s\ ^3P_1$ excited state requiring a wavelength $\lambda=286.3$ nm is used. For efficient detection the decay into the $5s^25p^2\ ^3D_2$ level at $\lambda=380.1$ nm was chosen.[27,28] The experimental setup has been described elsewhere;[17] we therefore restrict the description mainly to special features and alterations that were introduced for the tin experiments.

The evaporation of the tin samples required temperatures of about 2100 K which are much higher than those used previously in the apparatus. This temperature is considerably higher than that one required for evaporation of bulk tin. The reason possibly is that the samples are so small that the tin atoms are spread over the crucible in low concentration which seems to bind them more strongly to its surface. Therefore, a new heater of the electron bombardment type was developed. The anode is a vertically mounted tube made of high purity graphite. The crucibles are made of spectroscopically pure graphite so that practically no tin was detected with an empty crucible heated in the oven. The fluorescence detector was carefully shielded so that the stray light from the hot oven was reduced to a tolerable amount of 50 Hz count rate at operating conditions. It was of particular importance to construct the oven for long service intervals since it required a special handling procedure to repair it because of the radioactive contamination after use. The electrical heat power (2000 V; current up to 700 mA) is automatically stabilized by control of the cathode heater current to correct for anode-to-cathode backheating and other changes of the electrical characteristics. The atomic beam is collimated by an aperture in the crucible cover and an adjustable slit for a residual Doppler width that gives an observed full line width between 40 and 70 MHz. The natural width is 32 MHz.[22] Small samples are investigated with the slit fully open to gain in signal strength; the line width then was 70 MHz.

About 30% of the 380.1 nm fluorescence light is collected and focused onto the bialkali photocathode of a type 9635 B photomultiplier by THORN EMI. An interference filter with about 8 nm half width and 20% transmission is used to suppress stray light from different sources. The overall detection efficiency of the system including the atomic beam collimation losses is about one signal photon count per 2×10^5 sample atoms. 100 pg samples (5×10^{11} atoms) gave a signal peak count rate of 2 kHz lasting for about 10 sec. The smallest sample size for useful signals was 150 pg.

The continuous wave (cw) dye laser used was model CR 699-21 by Coherent with Rhodamine 6G dye dissolved in ethylene glycol and pumped by an argon ion laser. The single mode output power at 572.6 nm typically was 1.5 W for 7 to 9 W of single line (514.5 nm) pump power. To generate the 286.3 nm uv light required, the dye laser radiation was frequency doubled in a cooled ammonium dihydrogen arsenate (ADA) crystal.[17] The uv power obtained from 1.5 W of dye laser light was about 1.2 mW, which was sufficient to fully saturate the Sn transition. The fundamental visible and the harmonic uv light were separated by a quartz glass prism. All frequency measurements as well as frequency controls were done using the fundamental beam.

Two different dye laser tuning schemes were used. If a new isotope with unknown hyperfine structure was investigated, the laser was operated with its internal scan while the photon counts were accumulated in parallel by a multichannel counter. Thus rough line positions were found. To correct the results from such search runs for the scan nonlinearity, the equidistant resonances of a confocal 300 MHz resonator were recorded simultaneously.

In subsequent measurements the positions of all components were determined more accurately; the dye laser was then tuned under rf control. In this series of experiments one radioactive tin sample served to measure one component only. To make best use of the limited signal duration, the laser was first scanned in a narrow range only over this component. After the sample was exhausted the empty crucible was replaced with one that contained a reference isotope. To achieve the long term stability required for this procedure as well as the accuracy desired, rf laser tuning was employed. Instead of using the heterodyne technique as before,[17] a different rf method was applied that requires only one dye laser instead of two and which is superior in accuracy as compared to the earlier setup. The method[29–31] is based on rf-generated optical sidebands (see Fig. 1), which are generated by amplitude modulating the dye laser beam with a well known rf frequency; it defines the separation between the laser or carrier frequency and the side frequencies. An electro-optic modulator (model 1080 by Lasermetrics) is used for this purpose; it is driven by the output of a microwave synthesizer.

One of the sidebands is locked to an optical resonator with a free spectral range (FSR) of 300 MHz which is

fixed in frequency by an iodine stabilized HeNe laser. The sideband lock is accomplished by a feedback to the dye laser, i.e., the laser frequency is controlled such that the sideband chosen is held on the optical resonator peak. The peak lock is realized in the usual way by dithering the etalon at a rate of 4.6 kHz combined with phase sensitive detection. Any frequency change of the driving rf oscillation causes a dye laser frequency shift by precisely the same amount, thus defining the frequency scale. The rf synthesizer is operated under computer control; the laser is tuned in discrete steps of 5 or 10 MHz width across the resonance to be recorded. To speed up tuning and to reduce residual errors, the computer generates an analog feed-forward voltage that closely matches the expected control signal. In this way a tuning range of 1 GHz is accessible which was only limited by the synthesizer and rf power amplifier available. Since the dye laser light is frequency doubled, the corresponding tuning range of uv or atomic frequency level in this experiment is 2 GHz. The tuning range can be further doubled by locking the high or low frequency sideband to the reference resonator in turn.

To make full use of the scanning range a 2 GHz confocal etalon was sometimes placed in front of the 300 MHz reference cavity to filter the incoming light: the etalon serves to suppress the carrier and the unwanted sideband and to transmit the sideband used for locking. In this way undesired transmission coincidences with respect to the reference cavity are avoided that otherwise occur when the modulation frequency is a multiple of FSR/2=150 MHz. To facilitate locking the 2 GHz filter to the desired sideband, the sidebands are marked by a frequency modulation (4 MHz width at a speed of several kHz) applied to the modulating rf.[31] The filter lock utilizes a phase sensitive detection scheme which allows us to distinguish (i) the unmodulated carrier from the modulated side frequencies, and (ii) the two sidebands from each other since their frequency modulation is opposite in phase.

For the highly accurate measurements of stable isotopes, however, the extra 2 GHz filter was not used to reduce the complexity of the system. The coincidences were avoided in this operating mode by choosing the rf tuning ranges appropriately; this can be accomplished by making use of the dispersion of the gas inside the reference etalon housing by changing its pressure slightly.

III. SAMPLE PREPARATION

The samples of different isotopes were supplied in different ways. ^{113}Sn could be purchased, since it is a relatively long-lived isotope. ^{121}Sn, ^{121}Sn^{m}, ^{123}Sn, and ^{125}Sn were made from enriched stable Sn isotopes by neutron activation in the thermal flux of the two reactors of the Kernforschungsanlage at Jülich. For the neutron-deficient isotopes ^{110,111}Sn and the isomers ^{117}Sn^{m} and ^{121}Sn^{m}, targets of cadmium were irradiated with 10 MeV alpha particles using the internal beam of the Karlsruhe Isochronous Cyclotron.

After production the samples needed purification. This was particularly true for the reactor-made isotopes; this material underwent mass separation to concentrate the nuclei of interest. Thus, typically 200 pg of artificial tin were extracted from 20 mg of bulk material; the remaining stable Sn impurity content was about 50 ng. When Sn was made from cadmium, vacuum distillation was used. At a temperature of about 600 K the Cd target of about 30 mg is vaporized, leaving most of the Sn content back

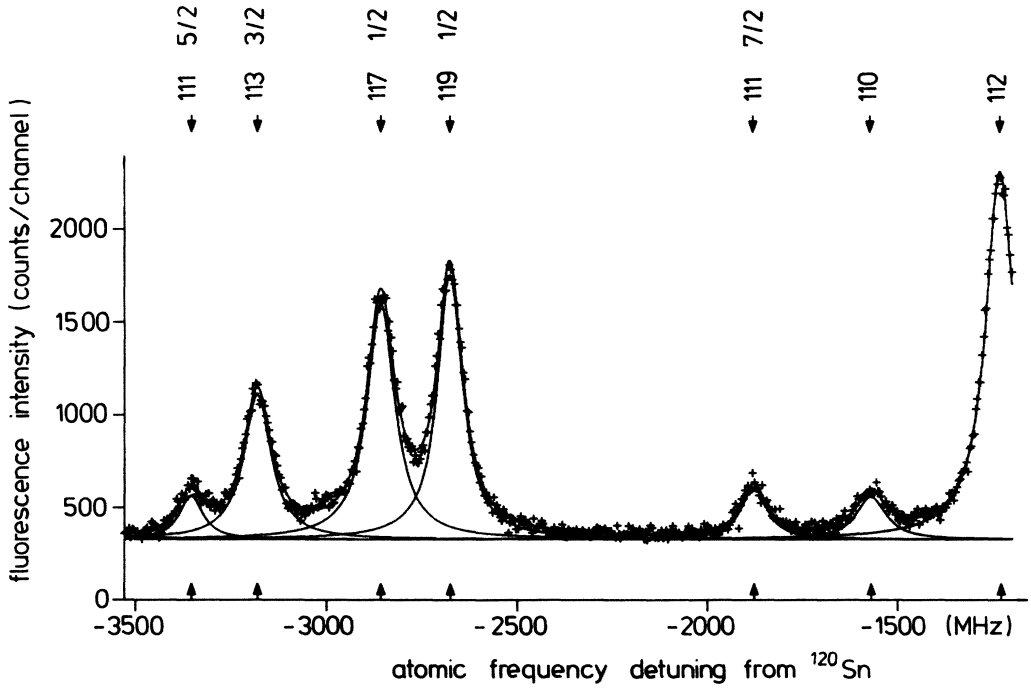

FIG. 2. Scan result for ^{111}Sn; ^{113,110}Sn and most of the ^{112}Sn are present since they are produced along with ^{111}Sn. ^{117,119}Sn are impurities.

TABLE I. Hyperfine component positions and the resulting isotope shift for tin isotopes and isomers together with the rms charge radius changes and the staggering parameters as derived thereof. ^{120}Sn was chosen as reference. F designates the total angular momentum quantum number of the atom in the upper electronic state. The half periods of the isotopes investigated range down to 35.3 sec (^{111}Sn).

Mass number A	Nuclear spin I	Total angular momentum F	Component position (MHz)	Isotope shift (MHz)	rms charge radius changes $\delta\langle r^2\rangle_{A,120}$ (fm^2)	Staggering parameter γ
110	0	1	−1566.5(7.0)	−1566.5(7.0)	−0.638(20)	
111	$\frac{7}{2}$	$\frac{5}{2}$	− 3351(10)			
		$\frac{7}{2}$	− 1876(10)	−1455(17)	−0.586(19)	0.67(13)
		$\frac{9}{2}$	20(40)			
112	0	1	−1218.29(15)	−1218.29(15)	−0.497(15)	
113	$\frac{1}{2}$	$\frac{1}{2}$	+ 3124.9(3.0)	−1079.3(2.3)	−0.438(14)	0.91(3)
		$\frac{3}{2}$	−3181.4(3.0)			
114	0	1	−900.68(15)	−900.68(15)	−0.367(11)	
115	$\frac{1}{2}$	$\frac{1}{2}$	+ 3589.24(15)	−804.92(12)	−0.322(10)	0.68(6)
		$\frac{3}{2}$	−3002.00(15)			
116	0	1	−576.04(15)	−576.04(15)	−0.236(7)	
117	$\frac{1}{2}$	$\frac{1}{2}$	+ 4314.02(20)	−471.43(12)	−0.189(6)	0.75(6)
		$\frac{3}{2}$	−2864.16(15)			
117m	$\frac{11}{2}$	$\frac{9}{2}$	+ 3482.2(4.0)			
		$\frac{11}{2}$	+ 89.5(2.0)	−483.3(1.8)	−0.192(6)	
		$\frac{13}{2}$	−3806.7(3.0)			
118	0	1	−270.24(15)	−270.24(15)	−0.112(4)	
119	$\frac{1}{2}$	$\frac{1}{2}$	+ 4828.36(20)	−179.59(12)	−0.070(2)	0.75(5)
		$\frac{3}{2}$	−2683.57(15)			
120	0	1	0	0	0	
121	$\frac{3}{2}$	$\frac{1}{2}$	−2687.3(3.0)			
		$\frac{3}{2}$	−1023.9(3.0)	+ 90.8(2.7)	+ 0.042(2)	0.83(4)
		$\frac{5}{2}$	+1760.0(5.0)			
121m	$\frac{11}{2}$	$\frac{9}{2}$	+ 4000.9(3.0)			
		$\frac{11}{2}$	+ 663.8(3.0)	+ 72.0(1.7)	+ 0.037(2)	
		$\frac{13}{2}$	−3241.7(3.0)			
122	0	1	+ 235.35(15)	+ 235.35(15)	+ 0.101(4)	
123	$\frac{11}{2}$	$\frac{9}{2}$	+ 4167.2(3.0)			
		$\frac{11}{2}$	+ 895.0(4.0)	+ 297.2(2.0)	+ 0.134(6)	0.71(7)
		$\frac{13}{2}$	−2979.4(3.0)			
124	0	1	+ 441.15(15)	+ 441.15(15)	+ 0.192(7)	
125	$\frac{11}{2}$	$\frac{9}{2}$	+ 4308.5(4.0)			
		$\frac{11}{2}$	+ 1098(20)	+ 504.3(7.5)	+ 0.225(9)	
		$\frac{13}{2}$	−2722(8)			

in the crucible. No mass separation was done with these samples since the loss is about 90%. This, however, leaves the tin impurity of the target material back in the sample. Therefore, in the case of ^{111}Sn, the ^{112}Cd target material used was vacuum distilled before irradiation to reduce the tin impurity. By the handling, however, the targets again were contaminated with several ng of natural Sn.

IV. MEASUREMENTS

The experiments were done in two steps. First a resonance search for a new isotope was performed which gave

a coarse value of the component positions; the internal laser scanning mode was used for these records. Figure 2 is a record of such scans for ^{111}Sn. Two of the three ^{111}Sn components are included in the scan range. The natural Sn contamination is visible as ^{117,119}Sn. All of the ^{113,110}Sn and most of the stable ^{112}Sn is artificial since it is produced together with the ^{111}Sn.

Most of the resonances thereafter were determined more accurately in a second measurement with rf sideband tuning. The radioactive samples were measured with a linewidth of 70 MHz and frequency steps of 10 MHz. The signal count rates were 1—5 KHz, the counting time then was chosen to be 150 msec per point. Background counts resulted mainly from scattered oven light (50 Hz at the full temperature of 2100 K) plus a rate of less than 70 Hz from the radioactivity. The stable isotopes were investigated at a width of 40 MHz; the count rates ranged from 10 to 700 kHz.

The digital records were evaluated fitting them by a Lorentzian profile. Sometimes a correction was required if a strong resonance of another isotope was close by, e.g., ^{114}Sn and ^{115}Sn ($F=\frac{3}{2}$) are obscured by ^{116}Sn and ^{117}Sn ($F=\frac{3}{2}$), respectively. To check the corrections, separate measurements were made with enriched samples for some but not all of the less abundant isotopes. This test showed that the correction is sufficiently accurate for the present purpose. There is, nevertheless, some remaining uncertainty as to the size of the correction since it depends on the line shape of the perturbing resonance far off the center. The actual line shape in the wings was not determined to high accuracy; in addition, it changed slightly with the collimation and the oven position. It is assumed, however, that the errors due to the use of a pure Lorentzian can be ignored. The component positions found in this way are summarized in Table I; ^{120}Sn is used as a reference isotope although for technical reasons in many cases the actual experiment was performed with some other reference isotope. The errors quoted are not the bare statistical ones as they result from the fits; these are quite small and would mostly be an underestimate of the true error. The uncertainties result from a detailed discussion of the actual experiment. For the group of experiments with radioactive samples, the main error stems from crucible motions which result in Doppler shifts. This is particularly true for those cases where the crucible was replaced to measure the stable reference isotope. A resonance was reproducible only to within ± 3 MHz under exchange of a crucible. The corresponding reproducibility of the crucible position is ± 200 μm. In addition, the fast temperature changes as the cold crucible is inserted and thereafter rapidly heated up causes two further errors: a crucible motion combined with a fast variation of the atomic beam intensity during the period of a single scan. Where these effects were important, the final error was further increased accordingly.

For the isotopes, ^{117}Sn^{m}, ^{121}Sn, and ^{125}Sn, one hyperfine component almost coincides with components of the stable isotopes ^{115,119,119}Sn, respectively, which might be present as an impurity with only a poorly known quantity in the radioactive sample. A detailed analysis of the combined signals allowed us to give the component position to within reasonable error limits.

A special problem was the component $F=\frac{9}{2}$ of ^{111}Sn. It could not be observed because of target contamination with natural Sn as mentioned above. The position of this component was estimated as follows: Assuming that B is 0 or very small as for the corresponding isotopes ^{121,123,125}Sn, the $F=\frac{9}{2}$ component lies close to the center of the strong ^{120}Sn line. If this is true, the ^{111}Sn component indeed is completely masked by ^{120}Sn. As a conservative guess of Q we therefore take $Q=0(0.12)$ b, which is reasonable in view of the Q values for ^{121,123,125}Sn. The component position then is $+20(40)$ MHz. This result is confirmed by measurements on a different optical transition of ^{111}Sn.[20]

As for the stable isotopes, the situation is quite different. They were finally measured under the best conditions achieved, i.e., without crucible or temperature changes. The single resonance results then scattered up to 500 kHz. To determine a spacing, the two resonance positions were measured many times in turn with a period of about one minute. The resulting spacings has a short term statistical scatter of only 50 kHz or less. The long term reproducibility, however, was worse; all independent results lie within an interval of ± 100 kHz but are sometimes statistically not consistent. We therefore quote in these cases a conservative error of ± 150 kHz which is $\pm 0.3\%$ of the observed line width. The problems associated with measurements to such small fractions of the line width and the nonstatistical errors of unknown origin found in several other examples will be discussed in a forthcoming paper.[30]

For the stable tin isotopes the present optical transition has been measured before with similar methods.[22] Some of the results are inconsistent with ours; this triggered a detailed investigation of possible systematic errors which led to the accuracy as described in the preceding paragraph. Among these studies are variations of the light power, the direction of the atomic and laser beams, the radio frequency used, the sideband combinations and the dye laser feedback circuit. The tests showed a reproducibility well within the 150 kHz limit given above. In addition to this internal consistency check we performed the same experiments with ^{57}Co; the test included the determination of well-known hyperfine splittings which were reproduced to within ± 50 kHz. The details will be given elsewhere.[30] It should be noted, however, that the discrepancies with Ref. 22 are far beyond the range where they are relevant with respect to the nuclear quantities to be extracted.

V. RESULTS AND DISCUSSION

From the results of the measurements given in Table I, isotopic and isomeric shifts as well as the values of the hyperfine structure constants (see Table II) have been derived. The experimental quantities are then evaluated in terms of nuclear charge radius differences and nuclear electromagnetic moments, respectively. Using the standard relations between the isotope shift $\delta\nu_{A',A}=\nu_{A'}-\nu_A$

TABLE II. Hyperfine splitting factors A and B with the corresponding nuclear moments μ_I and Q for tin isotopes and isomers. The values marked with an asterisk are taken from Refs. 33 and 34.

Mass number (A)	A factor (MHz)	B factor (MHz)	μ_I (μ_N)	Q_s (b)
111	+421.5(5.6)	0(19)	+0.617(8)	0(0.12)[a]
113	−4204.2(2.8)		−0.8791(6)	
115	−4394.16(14)		−0.91883(7)*	
117	−4785.45(17)		−1.00104(7)*	
117m	−606.7(4)	+53.3(3.3)	−1.3955(10)	−0.42(5)
119	−5007.95(17)		−1.04728(7)*	
121	+1112.4(1.7)	+2.3(2.1)	+0.6978(10)	−0.02(2)
121m	−603.3(4)	+18(4)	−1.3877(9)	−0.14(3)
123	−595.6(4)	−3.4(4.6)	−1.3700(9)	+0.03(4)
125	−586.0(9)	−12(21)	−1.348(2)	+0.09(17)

[a]This is an assumption.

and the mean square charge radius difference $\delta\langle r^2\rangle_{A',A}=\langle r^2\rangle_{A'}-\langle r^2\rangle_A$:

$$\delta\nu_{A',A}=F\delta\langle r^2\rangle_{A',A}+M(A'-A)/(A'A)\,, \tag{1}$$

we follow the procedure of Ref. 22 for determining the electronic parameters F and M. It is based on the result $\delta\langle r^2\rangle_{124,116}=+0.428(14)$ fm^2 (as obtained from the isotope shift of the K_α transition[32]) combined with isotope shift and hyperfine splitting results for $\lambda=645$ nm of Sn II. The above expression may be rewritten more specifically for the observed isotope shift of the $\lambda=286$ nm transition

$$\langle r^2\rangle_{A'}-\langle r^2\rangle_A=\delta\langle r^2\rangle_{A',A}=\frac{A'-A}{A'A}\frac{124\times116}{124-116}0.428(14)\ \text{fm}^2 + \frac{1\ \text{fm}^2}{3.3(0.3)\ \text{GHz}}\left[(\nu_{A'}-\nu_A)-\frac{A'-A}{A'A}\frac{124\times116}{124-116}(\nu_{124}-\nu_{116})\right]. \tag{2}$$

The resulting $\delta\langle r^2\rangle$ values are given in Table I and their variation with A is displayed in Fig 3. The quoted errors mainly arise from the uncertainty of the calibration value $\delta\langle r^2\rangle_{124,116}$. Figure 3 compares with the naive liquid drop estimate ($\langle r^2\rangle_A=\frac{3}{5}r_0^2A^{2/3}$ with $r_0=1.2$ fm) and the prediction of the (spherical) droplet model,[33,34] neglecting contributions from the variation of the mean square deformation $\langle\beta^2\rangle$ (or of the skin thickness of the nuclear charge distribution).

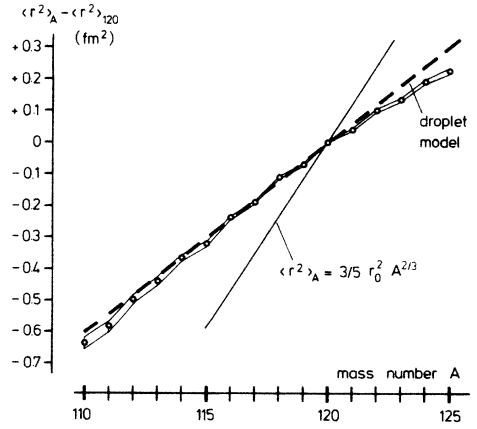

FIG. 3. The variation of the mean square charge radii of Sn nuclei with the mass number A as compared to the droplet model prediction. The systematic uncertainty arising from the calibration of the experimental data is indicated by an "error band" enclosing the data points.

For an estimate of the $\langle\beta^2\rangle$ influence, the variation of the mean square deformation is derived (within some systematic uncertainty) from the electromagnetic transition probabilities. The consideration of the $B(E2;0^+\rightarrow2_1^+)$ values of the even Sn nuclei leads to the conclusion that $\langle\beta^2\rangle$ is slightly increasing with decreasing neutron numbers.[20] An explicit account for such a variation would lift the droplet model curve for smaller A and deteriorate the good overall agreement between the observed data and the spherical droplet model. This feature is similarly observed for neutron-deficient Cd nuclei;[26] it may indicate that deformation effects play a minor role as compared to other nuclear structure effects.

In order to reveal the finer details, Fig. 4 displays the $\langle r^2\rangle$ changes for isotopes that differ by two units on the mass scale ($\delta\langle r^2\rangle_{A,A-2}$). The advantage of such a differential plot (Brix-Kopfermann plot) is that the uncertainty is smaller since δA is small. $\delta A=2$ is chosen in order to eliminate the odd-even staggering that dominates the changes with $\delta A=1$. The droplet model predicts a constant increase of $\delta\langle r^2\rangle$ with A.

The experimental results show a distinct drop at $N=64$ which may be attributed to the subshell closure when going from the $d_{5/2}$, $g_{7/2}$ to the $s_{1/2}$, $d_{3/2}$, and $h_{11/2}$ neutron orbits. This feature has already been shown in connection with studies of the mean square (ms) radii of

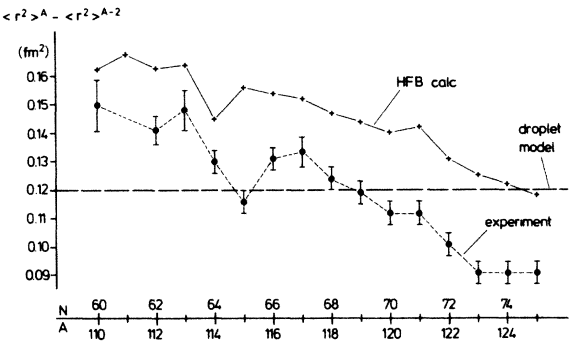

FIG. 4. The differential change $\delta\langle r^2\rangle_{A,A-2}$ of the mean square charge radii of Sn compared with theoretical results on the basis of the HFB theory (Ref. 11). The data for $N=60$ (^{108,110}Sn) were taken from Ref. 20.

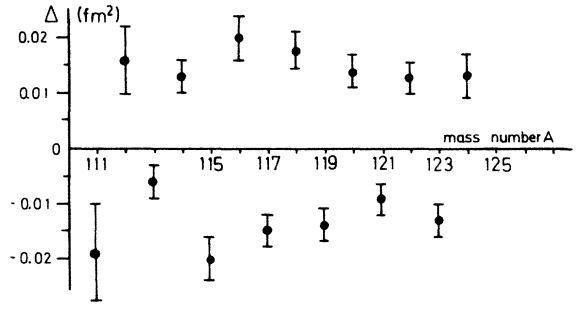

FIG. 5. The odd-even staggering of the mean square charge radii of Sn nuclei as represented by the quantity Δ as defined by Eq. (5).

stable even Cd isotopes.[26] In fact, microscopic nuclear structure calculations[11] on the basis of the Hartree-Fock-Bogoliubov (HFB) theory do predict such a dip, however, shifted by one unit on the mass scale. This discrepancy is unexplained at present.

The finest detail in the observed variation of $\langle r^2\rangle$ is the distinct odd-even staggering. This is traditionally represented by the parameter γ defined as

$$\gamma=2(\langle r^2\rangle_A-\langle r^2\rangle_{A-1})/(\langle r^2\rangle_{A+1}-\langle r^2\rangle_{A-1})\,, \tag{3}$$

which can be expressed more directly by the more accurate shifts $\delta\nu_{A',A}$

$$\gamma=2\frac{\delta\nu_{A,A-1}-M/(A(A-1))}{\delta\nu_{A+1,A-1}-2M/((A+1)(A-1))}\,, \tag{4}$$

thus eliminating the electronic parameter F and its uncertainty. The deviation of γ from unity is a measure for the degree and direction of the actual odd-even staggering. The values calculated with $M=671(480)$ GHz (taken from Ref. 22) are listed in Table I.

For considerations as discussed by Talmi,[35] an absolute measure of the staggering is more appropriate, namely the quantity

$$\begin{aligned}\Delta&=\langle r^2\rangle_A-\tfrac{1}{2}(\langle r^2\rangle_{A-1}+\langle r^2\rangle_{A+1})\\&=\tfrac{1}{2}(\delta\langle r^2\rangle_{A,A-1}-\delta\langle r^2\rangle_{A,A+1})\,,\end{aligned} \tag{5}$$

which is plotted in Fig. 5; it exhibits the different behavior of the even and odd Sn isotopes quite clearly.

For the odd isotopes and the isomers, the splitting constants A and B for the magnetic dipole and electric quadrupole hyperfine interaction have been determined. They are given in Table II. From A, the nuclear magnetic dipole moments μ_I were calculated using the well-known magnetic moments of ^{115,117,119}Sn.[36,37] The errors given for the unstable isotopes do not include a possible hyperfine anomaly since it is below 5×10^{-5} for the odd stable isotopes as results from a comparison with a precise g_I ratio determination.[38] The same has been found in two states of another electron configuration of tin.[23,38]

The magnetic moments reflect mainly the single particle properties of the ground and isomeric states investigated. The observed values are consistent with the Schmidt values. The deviations from the Schmidt values (actually up to 50%) may originate from core polarization and mesonic effects.

The extraction of the quadrupole moments from the observed B factors requires the value of the electric field gradient produced by the atomic electrons at the nuclear site or of the quantity $\langle r^{-3}\rangle_{5p}$. A rough estimate can be obtained from the spin orbit splitting of the $5p6s$ configuration. With the energy level data as taken from Ref. 27 the spin orbit interaction constant from standard formula[39,40] is found to be $\zeta=2659$ cm^{-1}. It follows[41] that $\langle r^{-3}\rangle_{5p}=9.45a_0^{-3}$. A more refined value has been calculated by Dembczynski and Rebel[42] using a semiempirical approach. Their result in terms of effective operator radial parameters is $\langle r^{-3}\rangle^{02}_{5p}=10.2(6)a_0^{-3}$. This value does not include Sternheimer core polarization type effects; the error given, however, does include the uncertainty due to this neglect. With the latter $\langle r^{-3}\rangle^{02}_{5p}$ it follows $Q_s=-0.0078(5)\times B(5p6s;{}^3P_1)$ b/MHz. The Q_s values given in Table II are calculated with this relation.

A discussion of the spectroscopic quadrupole moments in terms of the intrinsic nuclear deformation, by relating Q_s to the experimentally observed $B(E2)$ values or values of the ms deformation, respectively, is highly model dependent. In the case of the Sn nuclei with $\langle\beta^2\rangle^{1/2}\sim0.1$, the usual "strong coupling" relation (though sometimes applied in such cases) is hardly a basis for a meaningful comparison. The larger value of Q_s of the $\frac{11}{2}$ isomer ^{117}Sn^m as compared to the values of neighboring Sn nuclei must be considered together with a rather small isomer shift $\delta\langle r^2\rangle_{117m,117}$, thus indicating a rather complex relation between Q_s and the intrinsic nuclear deformation.

VI. CONCLUDING REMARKS

The low-lying energy level spectra of the Sn nuclei indicate a coexistence of states of distinct rotational character with vibrational structures. This interesting feature is common with other nuclei with proton or neutron numbers near a closed shell value. Generalized collective models like the Gneuss-Greiner model[43] or refined interacting boson models (IBM's) (Refs. 44 and 45) attempt to account for such mixed situations and provide the framework for a coherent discussion of the experimental

data: the level schemes, the transition probabilities, the electromagnetic moments, and the nuclear radii as well. The nuclear structure information specifically provided by the variation of the nuclear charge radii has recently been analyzed by Alonso, Arias, and Iachello[46,47] on the basis of the IBM-2 (Ref. 44) and IBFM-2 (Refs. 45) models, showing interesting nuclear structure aspects of the nuclear radius variation.

The main result of our present investigations is a set of precise experimental data on stable and radioactive Sn nuclides, which may serve at the basis of a detailed theoretical discussion in the framework of an advanced nuclear structure model. The observed trend in the Sn charge radii seems to be less affected by deformation effects (this is supported by the experimental quadrupole moments), however, we observed irregularities associated with more detailed shell effects (subshell closure at $N=64$) and a distinct odd-even staggering for which a quantitative microscopic explanation has been missing up to now.

We acknowledge the interest and valuable communications of J. Dembczynski, G. Huber, and I. Talmi, and thank B. Feurer for his technical assistance during the measurements.

---

*Present address: Department of Physics and Astronomy, Louisiana State University, Baton Rouge, LA 70803.

†Present address: Batelle-Institut e.V., D-6000 Frankfurt am Main 90, Federal Republic of Germany.

[1]D. N. Stacey, Rep. Prog. Phys. **29**, 171 (1966).

[2]B. Hoffmann, G. Baur, and J. Speth, Z. Phys. A **320**, 259 (1985).

[3]P. Jacquinot and R. Klapisch, Rep. Prog. Phys. **42**, 773 (1979).

[4]E.-W. Otten, in *Proceedings of the Fourth International Conference on Nuclei Far from Stability,* Helsingør, 1981, edited by P. G. Hansen and G. B. Nielson (CERN, Geneva, 1981), p. 3.

[5]*Proceedings of the Conference on Lasers in Nuclear Physics, Oak Ridge, Tennessee, 1982,* edited by C. E. Bemis, Jr. and H. K. Carter (Harwood-Academic, London, 1982).

[6]R. C. Thompson, Rep. Prog. Phys. **48**, 531 (1985).

[7]W. D. Myers and W. T. Swiatecki, Ann. Phys. (N.Y.) **55**, 395 (1969).

[8]E. Wesolowski, J. Phys. G **11**, 909 (1985).

[9]D. Berdichevsky and F. Tondeuer, Z. Phys. A **322**, 141 (1985).

[10]J. B. McGrory and B. A. Brown, see Ref. 5, p. 455.

[11]J. Dobaczewski, M. Flocard, and J. Treiner, Nucl. Phys. **A422**, 103 (1984).

[12]I. Talmi, Nucl. Phys. **A423**, 189 (1984).

[13]D. Zawischa, Phys. Lett. **155B**, 309 (1985).

[14]W. D. Myers and K. Schmidt, Nucl. Phys. **A410**, 61 (1983).

[15]H. Rebel, in *Proceedings of the XXth Winter School on Physics: Selected Topics of Nuclear Structure, Zakopane, Poland, 1985,* edited by R. Broda, Z. Stachura, and J. Styczén (Institute of Nuclear Physics, Jagiellonian University, Kraków, 1985).

[16]C. Thibault, F. Touchard, S. Büttgenbach, R. Klapisch, M. de Saint Simon, H. T. Duong, P. Jacquinot, P. Juncar, S. Liberman, P. Pillet, J. Pinard, J. L. Vialle, A. Pesnelle, and G. Huber, Phys. Rev. C **23**, 2720 (1981).

[17]R. C. Thompson, M. Anselment, K. Bekk, S. Göring, A. Hanser, G. Meisel, H. Rebel, G. Schatz, and B. A. Brown, J. Phys. G **9**, 443 (1983).

[18]M. Anselment, W. Faubel, S. Göring, A. Hanser, G. Meisel, H. Rebel, and G. Schatz, Nucl. Phys. **A451**, 471 (1986).

[19]M. Anselment, thesis, Universität Heidelberg, 1984; Kernforschungszentrum Karlsruhe Report 3797, 1984.

[20]H. Lochmann, thesis, Universität Mainz, 1985; Gesellschaft für Schwerionenforschung Report 85-8, and private communication.

[21]J. D. Silver and D. N. Stacey, Proc. R. Soc. London, Ser. A **332**, 139 (1973); **332**, 129 (1973).

[22]P. E. G. Baird, S. Blundell, G. Burrows, C. J. Foot, G. Meisel, D. N. Stacey, and G. K. Woodgate, J. Phys. B **16**, 2485 (1983).

[23]W. J. Childs, Phys. Rev. A **4**, 439 (1971).

[24]M. H. Prior, A. Dymanns, H. A. Shugart, and P. A. Van den Bont, Phys. Rev. **181**, 1665 (1969).

[25]A. Andl, K. Bekk, S. Göring, A. Hanser, G. Nowicki, H. Rebel, G. Schatz, and R. C. Thompson, Phys. Rev. C **26**, 2194 (1982).

[26]R. Wenz, A. Timmermann, and E. Matthias, Z. Phys. A **303**, 87 (1981), and references therein.

[27]C. E. Moore, *Atomic Energy Levels,* Natl. Bur. Stand. (U.S.) Circ. No. 467 (U.S. GPO, Washington, D.C., 1958), Sec. III.

[28]W. F. Meggers, C. H. Corliss, and B. F. Scribner, *Tables of Spectral-Line Intensities,* Natl. Bur. Stand. (U.S.) Circ. No. 145/I (U.S. GPO, Washington, D.C., 1975).

[29]B. Burghardt, W. Jitschin, and G. Meisel, Appl. Phys. **20**, 141 (1979); G. Meisel, Laser Optoelektronik **15**, 105 (1983); **15**, 245 (1983).

[30]M. Anselment, S. Chongkum, and G. Meisel, Kernforschungszentrum Karlsruhe Report 3969, 1985, p. 71 (unpublished).

[31]M. Anselment, S. Chongkum, H. Hoeffgen, and G. Meisel, Kernforschungszentrum Karlsruhe Report 3621, 1983, p. 65.

[32]S. Bhattacherjee, F. Boehm, and P. L. Lee, Phys. Rev. **188**, 1919 (1969).

[33]W. D. Myers, *Droplet Model of the Nucleus* (IFI/Plenum, New York, 1977).

[34]W. D. Myers, see Ref. 5, p. 437.

[35]I. Talmi, private communication.

[36]W. Proctor, Phys. Rev. **79**, 35 (1950).

[37]*Table of Isotopes,* edited by C. M. Lederer and V. S. Shirley, 7th ed. (Wiley, New York, 1978).

[38]H. Krüger, O. Lutz, A. Nolle, and A. Uhl, Z. Naturforsch. **27a**, 173 (1973).

[39]E. U. Condon and G. H. Shortley, *The Theory of Atomic Spectra* (Cambridge University, Cambridge, England, 1970).

[40]H. G. Kuhn, *Atomic Spectra,* 2nd ed. (Longmans, New York, 1969).

[41]H. Koperfermann, *Kernmomente* (Akademische, Frankfurt am Main, 1956).

[42]J. Dembczynski and H. Rebel, Kernforschungszentrum Karlsruhe Report 3815, 1984, p. 64.

[43]G. Gneuss and W. Greiner, Nucl. Phys. **A171**, 449 (1971).

[44]A. Asima, T. Otsuka, F. Iachello, and I. Talmi, Phys. Lett. **66B**, 205 (1977).

[45]N. Yoshida, A. Arima, and T. Otsuka, Phys. Lett. **114B**, 86 (1982).

[46]C. E. Alonos, J. M. Arias, and F. Iachello, Phys. Lett. **164B**, 241 (1985).

[47]F. Iachello, Nucl. Phys. **A358**, 89c (1981).